JOURNAL OF BACTERIOLOGY, May 2010, p. 2324–2334 Vol. 192, No. 9
0021-9193/10/$12.00 doi:10.1128/JB.00603-09
Copyright © 2010, American Society for Microbiology. All Rights Reserved.

Crystal Structure of Activated CheY1 from *Helicobacter pylori*▽

Kwok Ho Lam,[1] Thomas Kin Wah Ling,[2] and Shannon Wing Ngor Au[1]*

Centre for Protein Science and Crystallography, Department of Biochemistry and Molecular Biotechnology Program, Faculty of Science, The Chinese University of Hong Kong, Hong Kong,[1] and Department of Microbiology, The Chinese University of Hong Kong, Hong Kong[2]

Received 8 May 2009/Accepted 20 February 2010

Chemotaxis is an important virulence factor for *Helicobacter pylori* colonization and infection. The chemotactic system of *H. pylori* is marked by the presence of multiple response regulators: CheY1, one CheY-like-containing CheA protein (CheAY2), and three CheV proteins. Recent studies have demonstrated that these molecules play unique roles in the chemotactic signal transduction mechanisms of *H. pylori*. Here we report the crystal structures of BeF_3^--activated CheY1 from *H. pylori* resolved to 2.4 Å. Structural comparison of CheY1 with active-site residues of BeF_3^--bound CheY from *Escherichia coli* and fluorescence quenching experiments revealed the importance of Thr84 in the phosphotransfer reaction. Complementation assays using various nonchemotactic *E. coli* mutants and pull-down experiments demonstrated that CheY1 displays differential association with the flagellar motor in *E. coli*. The structural rearrangement of helix 5 and the C-terminal loop in CheY1 provide a different interaction surface for FliM. On the other hand, interaction of the CheA-P2 domain with CheY1, but not with CheY2/CheV proteins, underlines the preferential recognition of CheY1 by CheA in the phosphotransfer reaction. Our results provide the first structural insight into the features of the *H. pylori* chemotactic system as a model for *Epsilonproteobacteria*.

Helicobacter pylori is a spiral-shaped, Gram-negative, microaerophilic bacterium associated with gastritis, duodenal ulcers, gastric adenocarcinoma and mucosa-associated lymphoid tumors (43). About 50% of the world population is infected with this pathogen (6). The bacteria colonize the mucus layer covering the epithelial cell surface of the stomach, and this colonization step is necessary to establish a long-term infection. A number of *in vivo* mutagenesis studies have demonstrated the importance of bacterial motility in colonization and long-term infection in mouse and gerbil stomach models (11, 17, 27, 41, 47).

Chemotaxis has been well studied in enteric bacteria, such as *Escherichia coli* and *Salmonella enterica* serovar Typhimurium that evolved a two-component system composed of histidine kinase CheA and response regulator CheY (39, 45). Chemoreceptors sense an increasing concentration of repellent and promote autophosphorylation of CheA through the adaptor protein CheW. Activated CheA phosphorylates CheY by phosphoryl transfer from its histidyl residue to an aspartyl residue of CheY. Phosphorylated CheY (CheY-P) has an increased affinity for the flagellar switch protein FliM and consequently switches the motor from counterclockwise rotation (running) to clockwise rotation (tumbling). To enable a quick response to environmental changes, signal transduction from CheY to FliM is terminated by autodephosphorylation of CheY-P or by dephosphorylation via phosphatase CheZ. To move along concentration gradients, bacteria have chemoreceptors that undergo adaptation that is regulated by a methylation and demethylation system: for example, CheR methyltransferase and CheB methylesterase in *E. coli*.

Efforts to sequence prokaryotic genomes allow for comparisons of the diverse chemotaxis systems (28). *H. pylori* is similar to *E. coli* in the sense that it carries genes for CheY (HP1067), CheA (HP0392), CheW (HP0391), and a remote CheZ homolog (HP0170) (2, 40). However, *H. pylori* differs from *E. coli* in that it carries genes for multiple CheY-like proteins—a bifunctional CheA with a CheY-like domain (CheAY2) (*HP0392*) fused to the C terminus and three CheV (CheV1 [*HP0019*], CheV3 [*HP0393*], and CheV2 [*HP0616*]) genes, each consisting of an N-terminal CheW-like domain and a C-terminal CheY-like domain. Taken together with the lack of CheB and CheR homologs in the *H. pylori* genome, the mechanisms of chemotactic signal transduction and adaptation in *H. pylori* remain to be elucidated.

Structural studies on inactive and active *E. coli* CheY (EcCheY) and their complexes with FliM have revealed the molecular mechanisms of CheY phosphorylation and activation (8, 20, 21). (In the following text, "Hp" plus the gene name denotes *H. pylori*.) Phosphorylation is initiated by nucleophilic attack of Asp57 by phosphoryl phosphorus. Bound phosphate that is hydrogen bonded with Thr87 and Lys109 causes a displacement of the β4-α4 and β5-α5 loops and restricted the inward positioning of Tyr106 (8). The activation of EcCheY requires a divalent metal ion (Mg^{2+}/Mn^{2+}), which is coordinated by Asp13, Asp57, the backbone carbonyl of Asn59, the phosphoryl oxygen and two water molecules in the active-site pocket (20). Activated EcCheY binds the N-terminal fragment of FliM through its α4-β5-α5 interface. Recent nuclear magnetic resonance (NMR) study suggests that the transient interaction between the surface residues around the active-site pocket of *Thermotoga maritima* CheY and the middle FliM domain causes a displacement of $FliG_C$, which underlines the principle of motor switching (10).

* Corresponding author. Mailing address: Centre of Protein Science and Crystallography, Department of Biochemistry, Faculty of Science, The Chinese University of Hong Kong, Hong Kong. Phone: 852-31634170. Fax: 852-26035123. E-mail: Shannon-au@cuhk.edu.hk.

▽ Published ahead of print on 5 March 2010.

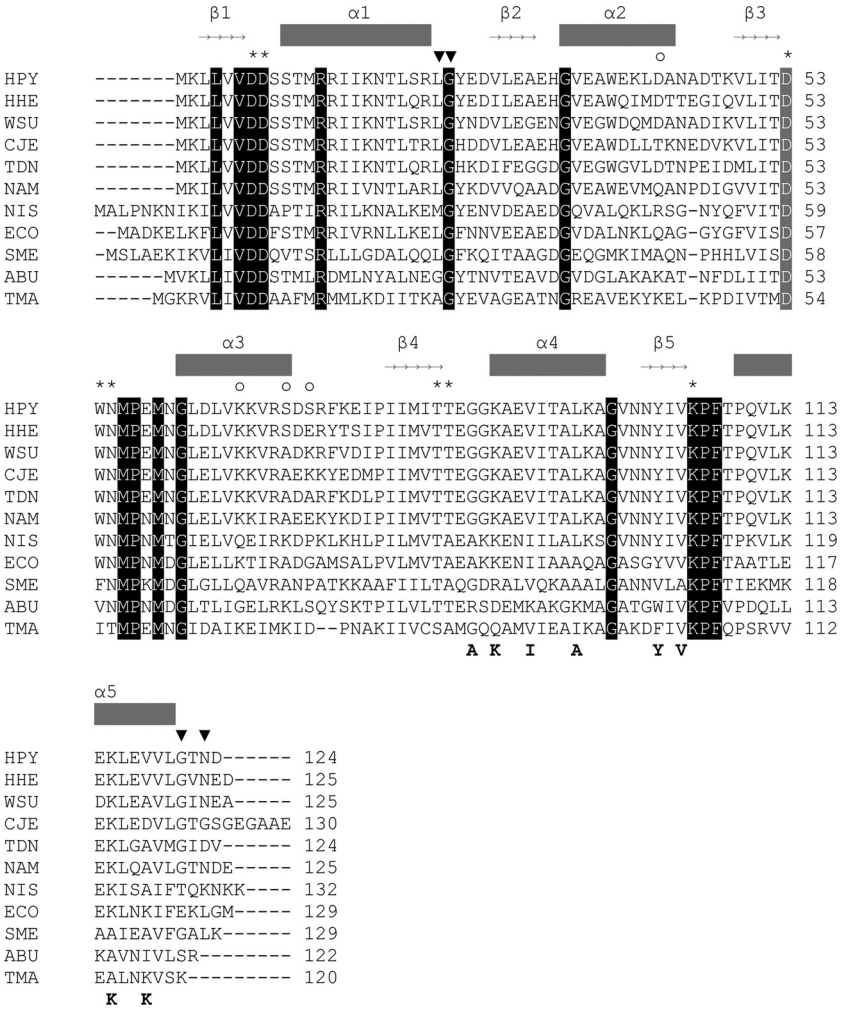

FIG. 1. Multiple sequence alignment of CheY1 from *Helicobacter pylori* 26695 (HPY), *Helicobacter hepaticus* (HHE), *Wolinella succinogenes* (WSU), *Campylobacter jejuni* NCTC11168 (CJE), *Sulfurimonas denitrificans* (TDN), *Nautilia profundicola* (NAM), *Nitratiruptor* sp. strain SB155-2 (NIS), *Arcobacter butzleri* (ABU), *Escherichia coli* K-12 MG1655 (ECO), *Sinorhizobium meliloti* (SME), and *Thermotoga maritima* (TMA) (18). Secondary structure elements of HpCheY1 are shown above the sequence alignment. Totally conserved residues are shaded. Phosphorylation site Asp53 is shaded in gray. Asterisks represent residues of the active-site pocket. ▼, residues responsible for the upshift of α5 in HpCheY1; ○, residues that varied between strains of *H. pylori*. Residues (in EcCheY) involved in $EcFliM_N$ binding are marked below the alignment (21).

HpCheY1 shares a moderately high level of amino acid sequence identity (46%) with EcCheY (ClustalW2), and both of these proteins exhibit a dephosphorylation rate of 0.035 s^{-1} (15, 37). Residues involved in phosphorylation and activation of EcCheY are conserved in HpCheY1 (Fig. 1), suggesting that HpCheY1 shares a similar activation mechanism. The HpCheY1 mutant is smooth-swimming biased, which is in line with the *E. coli* model (24). *In vitro* experiments showed that HpCheY1 is phosphorylated by CheA and interacts with FliM upon activation by acetyl phosphate (23). These data support the hypothesis that the biological function of HpCheY1 is comparable to that of EcCheY. However, the chemotactic regulatory mechanisms of *H. pylori* are different from those of *E. coli* in that the *H. pylori* genome carries multiple response regulators. All response regulators can be phosphorylated by CheA, which shows a preference for HpCheY1 (15). Interestingly, HpCheY1-P is able to transfer the phosphate back to HpCheA, and the phosphate moiety is transferred to HpCheY2, suggesting that *H. pylori* may exhibit retrophosphorylation, although this observation is not yet supported by *in vivo* evidence. CheV is proposed to be involved in one of the three adaptation mechanisms of *Bacillus subtilis* (32). However, the biological significance of HpCheVs is not as well understood. HpCheV1 mutant is nonchemotactic, and heterologous overexpression of HpCheV2 and HpCheV3 in *E. coli* inhibits swarming of the bacteria (31), suggesting that all three HpCheVs are associated with chemotaxis. Using fixed-time diffusion analysis, a more recent study showed that HpCheV1 and HpCheV2 mutants are biased toward smooth swimming, while HpCheV3 shows the opposite bias (24). Given that HpCheVs can be phosphorylated *in vitro* to different levels by HpCheA (15) and that HpCheV mutants show different extents of deficiency in colonizing mouse stomachs (24), it is likely that HpCheVs have distinct and important roles in chemotaxis. Furthermore, the different extent of phosphotransfer observed in *in vitro* studies indi-

cates that these proteins may display distinctive structural features (15, 31).

Despite the fact that the chemotactic system in *H. pylori* carries unique features and is critical for bacterial infection, none of the structures of the chemotactic proteins in *H. pylori* have been solved. In the present study, we solved the structure of BeF_3^--activated HpCheY1. We demonstrated the binding of BeF_3^- to HpCheY1 and the interaction between BeF_3^--HpCheY1 and HpFliM. Comparison of the BeF_3^--HpCheY1 and BeF_3^--EcCheY structures revealed a distinctive FliM binding surface. Further evidence of this distinctive binding surface was obtained by complementation assays using various nonchemotactic *E. coli* mutants. Our results have provided the first structural insight into the features of the *H. pylori* chemotactic system as a model for *Epsilonproteobacteria*. Comparison of the CheY structures from different bacteria has furthered our understanding of variations of chemotaxis pathways.

MATERIALS AND METHODS

Cloning, expression, and purification. Genes encoding HpCheY1 (HP1067), HpCheY2 (HP0392; residues 677 to 803) (15), HpCheV1 (HP0019), HpCheV2 (HP0616), HpCheV3 (HP0393), the HpCheA-P2 domain (HP0392; residues 110 to 261), and the $HpFliM_{NM}$ domain (HP1031; residues 1 to 237) were amplified from *H. pylori* strain 26695 genomic DNA and cloned into various expression vectors in order to obtain optimal expression level and solubility. HpCheY1, HpCheV1, and HpCheV2 were cloned into the pGEX-6P-1 expression vector. HpCheY2 and HpCheV3 were cloned into pET28m-sumo1 vector. HpCheA-P2 and $HpFliM_{NM}$ were cloned into pT7-7 vector with a C-terminal 8-histidine tag. Mutants HpCheY1/D53A and HpCheY1/T84A were generated using QuikChange site-directed mutagenesis kit (Stratagene) and verified by a commercial sequencing service (1st BASE).

Recombinant proteins were expressed in *Escherichia coli* strain BL21 and purified according to standard protocols (48). After transformation, cells were grown at 37°C until the optical density at 600 nm (OD_{600}) reached 0.4 to 0.6. Protein expression was induced by the addition of 0.3 mM IPTG (isopropyl-β-D-thiogalactopyranoside) and the cells were further grown at 16°C or 25°C for 16 h. Cell pellet was resuspended in lysis buffer (10 mM Tris-HCl, pH 7.8, and 500 mM NaCl) and lysed by sonication. Cell lysate was clarified by centrifugation (40,000 × *g*, 1 h and 4°C) and the supernatant was incubated with preequilibrated affinity resin for 2 h at 4°C with gentle shaking. After washing the beads with the lysis buffer, the glutathione *S*-transferase (GST) tag was cleaved by Prescission protease, when necessary. For the His-sumo1 fusion protein, the tag was removed by incubation with sumo protease SENP1 in a mass ratio of 1:100 at 37°C for 30 min (48). The eluted proteins were then further purified by size exclusion chromatography using Superdex 75 or Superdex 200 equilibrated with buffer containing 10 mM HEPES (pH 7.0) and 150 mM NaCl.

Nickel pull-down assay. (i) CheAP2-CheY interaction assay. An aliquot of 25 μl nickel-nitrilotriacetic acid (NTA) resin (Qiagen) was pipetted into a 1.5-ml Eppendorf tube and centrifuged (3,300 × *g*, 10 s, and 4°C). The beads were washed 3 times with binding buffer containing 20 mM imidazole (pH 7.0), 150 mM NaCl, and 2 mM $MgCl_2$. It was followed by the addition of 1 ml purified HpCheA-P2-8×His protein solution in a concentration of 0.1 mg/ml. The mixture was incubated at 4°C for 1 h with gentle shaking. The beads were washed three times with the binding buffer followed by the addition of purified HpCheY1, HpCheY2, HpCheV1, HpCheV2, and HpCheV3 in a molar ratio of 1:1. The mixture was incubated for another 1 h at 4°C. The beads were washed three times with the buffer and then resuspended in 25 μl of 2× SDS-PAGE gel loading buffer and heated to 90°C for 8 min. The samples were subjected to SDS-PAGE analysis and Coomassie blue staining.

(ii) FliM-CheY interaction assay. The pull-down experiment was performed as described previously with modifications (23). All experimental steps were performed at 25°C. $HpFliM_{NM}$ was immobilized onto nickel-NTA resin preequilibrated with buffer containing 10 mM HEPES (pH 7.6), 5 mM $MgCl_2$, 250 mM KCl, 0.15% Tween 20, and 20 mM imidazole. After incubation for 1 h, the beads were washed for 3 times. HpCheY1 and HpCheY1/D53A were preincubated with 0.75 mM $BeCl_2$ and 18 mM NaF for 10 min before being incubated with the immobilized $HpFliM_{NM}$ for 15 min. The beads were washed twice, boiled with gel loading buffer, and subjected to SDS-PAGE analysis.

Size exclusion chromatography. Purified HpCheY1 and HpCheV3 were individually mixed with HpCheA-P2-8×His in a buffer containing 10 mM HEPES (pH 7.4), 150 mM NaCl, and 2 mM $MgCl_2$. The mixture was incubated on ice for 30 min. Individual proteins or mixtures were applied to a Superdex 200 HR 10/30 gel filtration column (GE Healthcare Bio-Sciences Corp.) and eluted at 0.6 ml/min with the same buffer. Eluted proteins were subjected to SDS-PAGE analysis and Coomassie blue staining.

Fluorescence spectroscopy. Fluorescence measurement was carried out using a Perkin Elmer 50B spectrofluorimeter. Fluorescence was measured at an excitation wavelength of 293 nm and an emission wavelength of 341 nm with slit widths of 3 nm and 6 nm for excitation and emission, respectively. All reactions were carried out at 25°C. Equilibrium titrations of HpCheY1, HpCheY1/D53A, and HpCheY1/T84A by acetyl phosphate were carried out in a buffer containing 20 mM sodium phosphate (pH 7.5), 50 mM NaCl, and 2 mM $MgCl_2$. The final concentrations were 1 μM for HpCheY1s and 0.3 to 10 mM for acetyl phosphate. Titration of HpCheY1 or HpCheY1/D53A with BeF_3^- was performed by sequential addition of NaF to the protein solution containing 10 μM $BeCl_2$. The final concentration of NaF was set to 0 to 5 mM. Fluorescence changes upon addition of small molecules were monitored until the fluorescence signal stabilized. The fluorescence values were corrected for dilution. K_m was determined as described previously (25, 31, 36). Acetyl phosphate concentration was plotted versus $(I_o - I)/(I - I_{inf})$, where I_o is initial fluorescence intensity, I is the intensity at the corresponding acetyl phosphate concentration, and I_{inf} is the intensity at the saturating concentration. From the plot, the reciprocal of the slope of the line corresponds to the K_m value. According to proposed reaction scheme (25), shown as follows, $K_m = K_s\, k_3/k_2$

$$\mathrm{CheY1} + \mathrm{Ac{\sim}P} \overset{K_s}{\longleftrightarrow} \mathrm{CheY1 \cdot AcP} \overset{k_2}{\longrightarrow} \mathrm{CheY1 \cdot P} \overset{k_3}{\longrightarrow} \mathrm{CheY1} + \mathrm{P_j}$$

where K_s is the equilibrium dissociation constant between CheY1 and acetyl phosphate and k_2 and k_3 are the phosphorylation and dephosphorylation rate constants, respectively.

Swarming assay. *E. coli* motility wild-type strain RP437 and chemotaxis mutant strains RP1616 (Δ*cheZ*) and RP5232 (Δ*cheY*) were gifts from J. S. Parkinson (29). The complementation assay was performed by individual transformation of pTrc99a, pTrc99a-HpCheY1, and pTrc99a-HpCheY1/D53A in strain RP437 and chemotaxis mutants RP1616 (Δ*cheZ*) and RP5232 (Δ*cheY*). An aliquot of a 1-μl overnight culture was spotted onto 0.4% TB soft agar (1% tryptone, 0.5% NaCl, and 0.5% glycerol, 0.4% agar). Ampicillin (100 μg/ml) and IPTG (isopropyl-β-D-thiogalactopyranoside; final concentration of 0.05, 0.1, or 0.5 mM) were added when necessary. The diameter of the chemotactic rings was measured after incubation at 30°C for 7 h.

Immunoblotting. An aliquot of a 1-μl overnight culture of *E. coli* strains RP437 and RP1616 (Δ*cheZ*), RP9535 (Δ*cheA*), and RP5232 (Δ*cheY*) transformed with the recombinant plasmids were added to 3 ml of TB medium with 0, 0.05, 0.1, and 0.5 mM IPTG when necessary. Cells were grown overnight at 30°C with vigorous shaking. The cells were harvested and washed with a buffer containing 10 mM HEPES (pH 7.4) and 150 mM NaCl. The samples were subjected to SDS-PAGE analysis followed by immunoblotting with polyclonal anti-HpCheY1 antibody (Invitrogen).

Crystallization condition of HpCheY1. Initial crystallization trials were performed by Crystal Screens I and II from Hampton Research (Hampton Research, Aliso Viejo, CA) using the sitting drop vapor diffusion method. Diffraction-quality crystals of HpCheY1 grown at 16°C were obtained from an optimized screening condition containing 0.1 M sodium acetate (pH 5.0), 0.2 M ammonium sulfate, 35% MPEG2000, and 1 mM $MgCl_2$. Crystals of HpCheY1/D53A and T84A were grown under a similar condition. For BeF_3^--HpCheY1, the crystals were grown in crystallization buffer containing 0.1 M sodium acetate (pH 5.0), 0.05 M ammonium sulfate, 1.6 mM $BeCl_2$ (1:10 CheY1-$BeCl_2$) and 16 mM NaF.

Data collection and processing. A 1.8-Å X-ray data set for HpCheY1 crystal, 2.2-Å X-ray data set for BeF_3^--HpCheY1 crystal, 2.2-Å X-ray data set for HpCheY1/D53A crystal, and 1.7-Å X-ray data set for HpCheY1/T84A crystal were collected at 100 K using a Rigaku MicroMax 007 X-ray generator at the Centre for Protein Science and Crystallography, The Chinese University of Hong Kong, and recorded on a RAXIS IV++ image plate. For each crystal, crystallization buffer containing 15% glycerol was used as a cryoprotectant. Images were processed using *Mosflm* (22) and scaled and reduced with *SCALA* from the CCP4 suite (5). All of the four protein structures were in spacegroup C2, and unit cell parameters and statistics for the data collected are summarized in Table 1.

TABLE 1. Diffraction data and refinement statistics of CheY

Parameter	Result for[a]:			
	CheY	CheY-BeF_3^-	CheY D53A	CheY T84A
X-ray data statistics				
Spacegroup	C2	C2	C2	C2
Unit cell				
a, b, c (Å)	70.3, 38.5, 38.9	70.3, 38.4, 38.7	70.3, 38.1, 38.6	70.4, 38.1, 39.0
α, β, γ (Å)	90.0, 107.0, 90.0	90.0, 107.0, 90.0	90.0, 107.4, 90.0	90.0, 107.6, 90.0
Resolution range (Å)	37.2–1.8 (1.9–1.8)	33.3–2.2 (2.28–2.2)	36.9–2.2 (2.28–2.2)	23.08–1.7 (1.76–1.70)
No. of observations	33,157	20,879	18,875	38,199
No. of unique reflections	9,175	4,888	4,993	10,972
Redundancy	3.6 (3.6)	4.3 (4.4)	3.8 (3.8)	3.5 (3.3)
Completeness (%)	98.1 (96.1)	95.3 (91.8)	98.5 (97.0)	99.9 (100.0)
R_{merge}	0.031 (0.072)	0.019 (0.029)	0.082 (0.240)	0.033 (0.199)
Mean $I/\sigma I$	30.3 (15.4)	55.1 (39.0)	10.6 (4.5)	14.2 (5.2)
Refinement statistics				
Resolution	37.16–1.8	33.46–2.4	36.89–2.2	23.08–1.7
R value	14.67	15.14	17.78	17.35
R_{free} (5% of data)	18.61	22.01	23.11	20.28
No. of atoms refined				
Protein	966	966	963	964
Water/SO_4/Mg/BeF_3	143/2/2/0	60/1/2/1	68/2/1/0	132/2/2/0
RMSD from ideal geometry				
Bond lengths (Å)	0.011	0.013	0.020	0.014
Bond angles (°)	1.37	1.40	1.87	1.42
Ramachandran plot	91.8/7.3/0.9	91.8/7.3/0.9	90.9/8.2/0.9	90.9/8.2/0.9

[a] Values in parentheses are for the last resolution shell. $R_{merge} = (\Sigma h \Sigma j \mid <I(h)> - I(h)j|/\Sigma h \Sigma j <I(h)>)$, where $<I(h)>$ is the mean intensity of symmetry-equivalent reflections. R value $= \Sigma||F_{obs}| - |F_{calc}||/\Sigma|F_{obs}|$, where F_{obs} and F_{calc} are the observed and calculated structure factors, respectively. The distribution of the residues in the most favored/additionally allowed regions of the Ramachandran plot was evaluated by PROCHECK (19).

Structure determination and refinement. The HpCheY1 structure was solved by molecular replacement using a molecule of EcCheY (Protein Data Bank identification [PDB-ID] no. 3CHY) as a search model. Molecular replacement program *PHASER* (26) in CCP4 suite was performed with data in the resolution range 15 to 3.0 Å. For the other three structures, the refined structure of HpCheY1 was used as a search model. The randomly selected 5% of data was reserved for the R_{free} calculation for all the three structures. Rounds of refinements and manual rebuilding were performed by using the programs *REFMAC* and *COOT* (5, 12), respectively. The electron density maps from $2F_o-F_c$ and F_o-F_c calculations were used for model building, and for all of the structures, strong electron density was found close to the active-site Asp 53. We modeled them as sulfate molecules for HpCheY1, HpCheY1/D53A, and HpCheY1/T84A structures. For the CheY1 crystal grown in the presence of beryllium and sodium, a beryllium fluoride molecule was modeled in the active site. The Ramachandran plots drawn by the program PROCHECK (19) showed that over 88% of all residues in the four CheY1 structures fall within the most favored region.

Protein structure accession numbers. Coordinates have been deposited in the Protein Data Bank under PDB-ID no. 3GWG, 3H1E, 3H1F, and 3H1G.

RESULTS AND DISCUSSION

HpCheY1 is activated by beryllofluoride. HpCheY1-P has a short half-life (20 s), precluding structural analysis of HpCheY1-P (15). BeF_3^- is known to form a persistent complex with response regulators by mimicking an acyl phosphate (4, 20). In prior to the structure-function analysis, the binding of BeF_3^- to HpCheY1 was examined by steady-state fluorescence quenching. A reaction mixture containing 1 μM HpCheY1 and 10 μM $BeCl_2$ was titrated by sequential addition of 0.5 M NaF to a final concentration of 0 to 5 mM. HpCheY1 contains two tryptophan residues (Trp38 and Trp54). The conserved Trp54 residue in EcCheY has been used to report the binding of small molecules to the active-site pocket (25). The fluorescence of Trp38 is not affected by this binding because it is located at helix 2, and no conformational change in helix 2 was reported upon phosphorylation (20). As shown in Fig. 2A, the tryptophan fluorescence of HpCheY1 decreased upon addition of increasing amounts of NaF and was almost saturated at 4 mM NaF. The HpCheY1/D53A mutant, a nonphosphorylatable analog, showed no decrease in fluorescence, suggesting that HpCheY1 binds BeF_3^- and that an aspartic residue is necessary for the binding. As a control, phosphorylation of HpCheY1 by acetyl phosphate was monitored, and comparable decreases in fluorescence were observed for the wild type and the D53A mutant (Fig. 2B).

Activated CheY has an enhanced affinity for FliM (49), and a recent study demonstrated the binding of HpCheY1-P to HpFliM upon activation by acetyl phosphate (23). To further verify that HpCheY1-BeF_3^- mimics HpCheY1-P, the interaction of HpCheY1-BeF_3^- with HpFliM was examined by an *in vitro* pull-down assay. HpCheY1 and $HpFliM_{NM}$ (consisting of the N-terminal and middle domains fused to a C-terminal His_8 tag) were purified to greater than 95% purity. $HpFliM_{NM}$ was immobilized on Ni-NTA resin, followed by incubation with wild-type HpCheY1 or the D53A mutant with or without BeF_3^-. As shown in Fig. 2C, only wild-type HpCheY1 complexed with BeF_3^- showed a stable interaction with $HpFliM_{NM}$, suggesting that HpCheY1-BeF_3^- mimics the activated form of HpCheY1 in the interaction with $HpFliM_{NM}$.

Description of the HpCheY1 structure. The crystal structure of HpCheY1-BeF_3^- was solved at a resolution of 2.4 Å, with R = 15.14% and R_{free} = 22.01%. The overall structure retained a $(\beta/\alpha)_5$ fold typical of response regulators. From a *DALI* search (13), HpCheY1 showed high structural homology to EcCheY/D13K/Y106W (PDB-ID 1U8T) (9) and to BeF_3^--

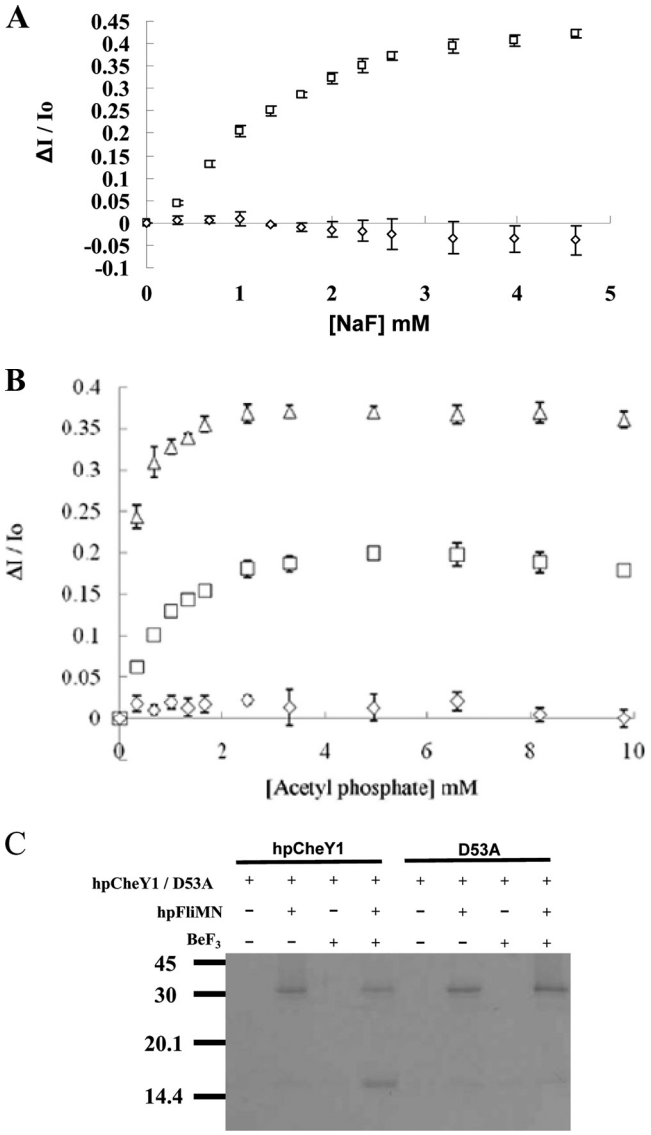

FIG. 2. Activation of HpCheY1 by beryllofluoride. Fluorescence spectroscopy analysis of HpCheY1 (□), HpCheY1/D53A (◇), and HpCheY1/T84A (△) upon addition of sodium fluoride (A) and acetyl phosphate (B) is plotted. Fluorescence changes were plotted as $\Delta I/I_o$ against concentration, where ΔI represents the cumulative changes in fluorescence intensity at the corresponding small molecule concentrations and I_o is fluorescence intensity without addition of small molecules. (C) Pull-down study of HpCheY1 with HpFliM. Purified $HpFliM_{NM}$ in 0.1 mg/ml was immobilized on prewashed resin. HpCheY1 or the D53A mutant in a 2:1 molar ratio to $HpFliM_{NM}$ was incubated with immobilized $HpFliM_{NM}$ with or without BeF_3^- at 25°C for 15 min.

bound EcCheY/F14E/N59M/E89L (PDB-ID 3F7N) (30), with Cα root mean square deviation (RMSD) values of 0.776 Å and 0.684 Å, respectively. Alignment of the amino acid sequences of HpCheY1 proteins from different *H. pylori* strains revealed four variable residues: Asp42 positioned at α2 (Asn in Shi470), Lys66 at α3 (Ile in Shi470), Ser70 at α3 (Ala in P12/J99/Shi470), and Ser72 at the α3-β4 loop (Asn in J99 and Glu in Shi470). These residues are located on the distal side of the active site, which may not be directly involved in activation or FliM binding (Fig. 1).

Structural alignment with BeF_3^--EcCheY revealed that the conformation of most of the active site residues and of the hallmark residues for CheY activation, including Thr83 and Tyr106, aligned well when the structures of BeF_3^--HpCheY1 and BeF_3^--EcCheY were superimposed. This suggests that HpCheY1 shares a similar activation mechanism (8). On the other hand, a number of structural differences were noted. These differences were clustered at the α2-β3 loop, helix 5, and the C-terminal loop (Fig. 3A). The former one corresponded to an insertion of Ala45 in the HpCheY1 sequence; however, no distortion of the overall protein fold, especially the active site pocket, was observed. Interestingly, helix 5 of HpCheY1 was five residues shorter and was upshifted by approximately 3.4 Å. The movement of helix 5 may be related to a combination of effects from residues Gly121, which causes an early termination of the helical structure, and Asn123, which is hydrogen bonded to residues in the α1-β2 loop (backbone NH of Asn123 to the backbone carbonyl of Leu23 and Nδ of Asn123 to the backbone carbonyl of Gly24), leaving the C-terminal loop positioned in a rigid conformation. Gly121 is conserved in most *Epsilonproteobacteria* and in some other proteobacteria (Fig. 1). The corresponding Gly126 in the CheY2 structure from *Sinorhizobium meliloti* (PDB-ID no. 1P6U) also causes early termination of the helical structure, but the C-terminal loop flips to the other side (33). Sequence alignment of CheYs showed that the number and types of residues following Gly121 are variable. Residue Asn123 is only conserved in some related bacteria species. We speculate that the helical upshift of CheY1 is a unique feature in *H. pylori* and some closely related species. These structural discrepancies, which could not be predicted from the multiple sequence alignment, in fact provide insights into the molecular interaction with FliM. Analysis of the surface potential of HpCheY1 and EcCheY clearly demonstrated that although the hydrophobic surface of helix 4 is retained, the electropositive patch contributed by helix 5 for the FliM interaction was much weaker in the HpCheY1 structure (data not shown).

We also attempted to solve the structure of apo-HpCheY1. To our surprise, a tetrahedral positive electron density was observed in the active-site pocket during model building (Fig. 4A). The electron density shown in the active-site pocket of the 1.8-Å "apo-HpCheY1" structure was interpreted as a sulfate ion because of the addition of 200 mM ammonium sulfate in the crystallization medium. The structure of the HpCheY1/D53A mutant was also solved to a resolution of 2.2 Å. However, the sulfate moiety was still found in the active-site pocket of HpCheY1/D53A. The overall structures of sulfate-bound HpCheY1 and HpCheY1/D53A were almost identical to the HpCheY1-BeF_3^- structure, including the α4-β4 loop and Tyr102, with Cα RMSD values of 0.147 Å and 0.199 Å, respectively, suggesting that sulfate-bound HpCheY1s may represent an activated form. We investigated whether the nonphosphorylatable D53A analog of HpCheY1 can be "activated" by high concentration of ammonium sulfate. We found that sulfate binds HpCheY1/D53A *in vitro* as the tryptophan fluorescence intensity of HpCheY1/D53A decreased by 30% upon titration with ammonium sulfate (data not shown). The titration was saturated when the concentration of ammonium sulfate reached around 360 mM, with a calculated K_m of 176 ± 21 mM. To further investigate whether sulfate enhanced the abil-

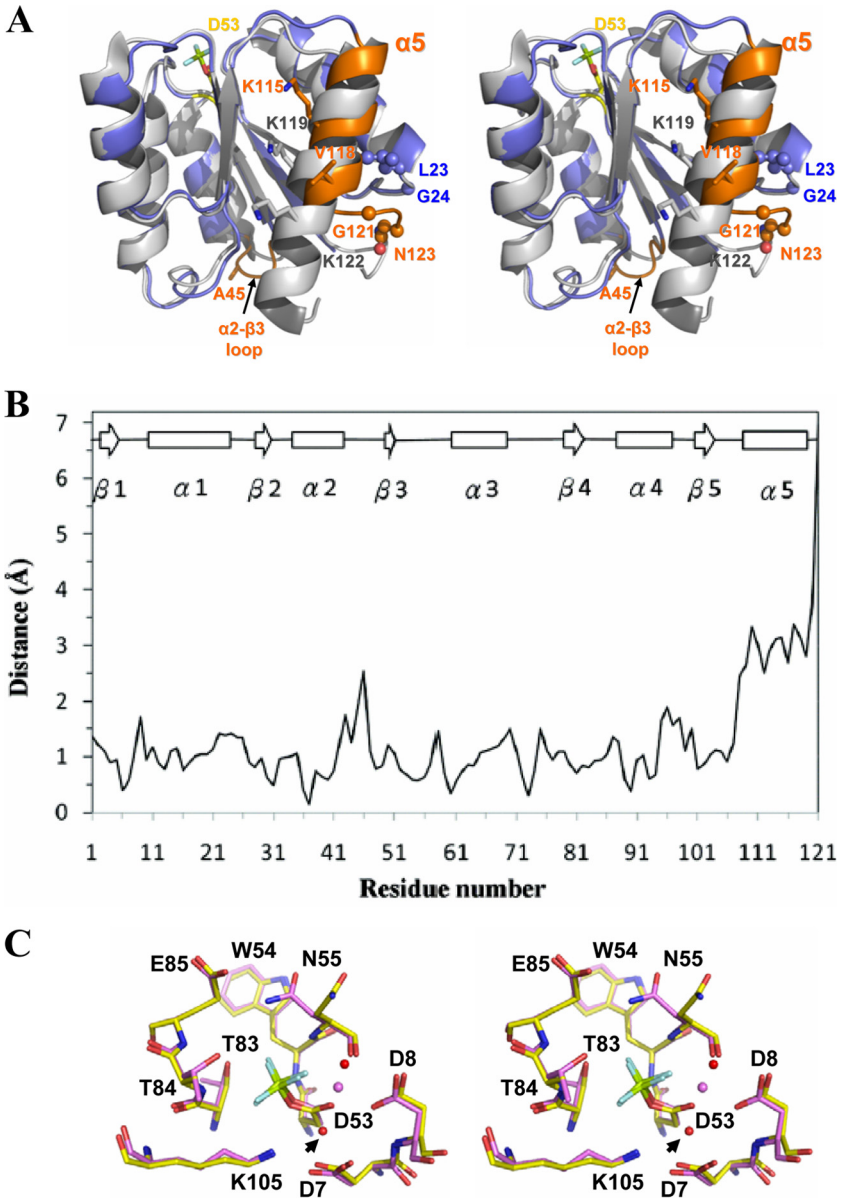

FIG. 3. (A) Structural superimposition of BeF_3^--HpCheY1 (blue) and BeF_3^--EcCheY (white) (PDB-ID no. 1FQW) highlights the features of the HpCheY1 α2-β3 loop, α5, and the C-terminal loop (orange). Insertion at Ala45 and the major differences in residues involved in $EcFliM_N$ binding (Lys119 and Lys122 in EcCheY and Lys115 and Val118 in HpCheY1) are shown as sticks. Residues that contributed to α5 upshift are shown as spheres. Phosphorylation site Asp53 of HpCheY1 bonded with BeF_3^- is shown as a stick. (B) Differences in Cα positions between BeF_3^--bound HpCheY1 and EcCheY. The least-square superposition program LSQKAB (CCP4) was used to superimpose HpCheY1 (residues 1 to 121) with EcCheY (residues 6 to 125) and to calculate individual Cα distances. Residue 45 of HpCheY1 was not aligned from the calculation and is not shown on the plot. Residues are numbered according to HpCheY1 sequence. Secondary structure is shown above the plot. (C) Stereo superimposition images of BeF_3^--HpCheY1 (pink) and EcCheY (yellow) on the basis of structural alignment using Pymol. Residues in the active-site pocket are labeled. Metal ions (Mg^{2+} in HpCheY1) and two water molecules (red sphere) (from BeF_3^--HpCheY1) involved in coordinating the metal ion (pink sphere) are shown. An arrow indicates the water molecule coordinated by Asp7.

ity of the D53A mutant to interact with HpFliM, an *in vitro* pull down assay was performed in the presence of 200 mM ammonium sulfate (without KCl). HpCheY1/D53A showed enhanced binding to $HpFliM_{NM}$ in the presence of ammonium sulfate (data not shown), but not in BeF_3^- (Fig. 2C), agreeing with the structural information of SO_4^{2-}-bound HpCheY1/D53A in an activated configuration. Note that the interaction is of no known physiological relevance given the high concentration of ammonium sulfate.

A sulfate molecule positioned close to the active-site pocket has been reported in the crystal structure of apo-EcCheY (PDB-ID no. 3CHY), in which the SO_4^{2-} was hydrogen bonded with Lys109 Nε and Asn59 Nδ (in the *E. coli* sequence) (44). However, our results show that the hydrogen bond net-

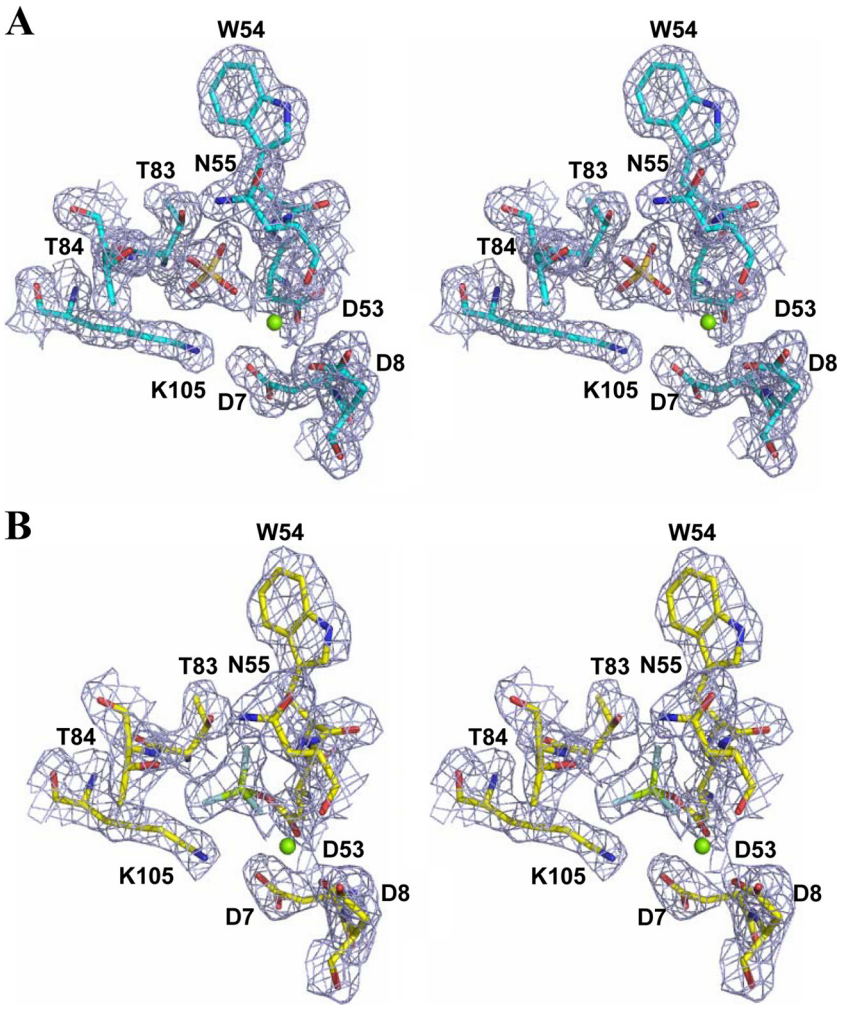

FIG. 4. Stereo view of the active site of HpCheY1 showing the $2Fo-Fc$ electron density around SO_4^{2-} (A) and BeF_3^- (B) moieties contoured at 1.0 σ (7). Active-site residues are labeled and shown as sticks. Mg^{2+} is shown as a sphere.

working of SO_4^{2-} with the active-site residues in HpCheY1 was comparable to that found in BeF_3^--HpCheY1. An "inward" orientation of the side chain of Asp53, in which the side chain is flipped toward the protein core, was noted in SO_4^{2-}-bound HpCheY1 (Fig. 4). Such rearrangement is very likely induced by the charge-charge repulsion upon sulfate binding. The flipping of Asp53 is stabilized by hydrogen bond formation with its own peptide NH (2.85 Å), with the peptide NH of Trp54 (3.47 Å), with the peptide NH of Asp8 (3.41 Å), and with Mg^{2+} (2.44 Å).

Comparison of the active-site pockets. The active-site residues of HpCheY1 aligned well with those in EcCheY, except for the flipping of the Asn55 side chain and the replacement of Thr84 with an alanine in the EcCheY sequence (equivalent to Ala88 in EcCheY). The side chain of the conserved Asn55 in HpCheY1 was flipped to an alternative conformation and was hydrogen bonded with the carboxylate Oε of Glu85 (2.9 Å). The coupling of Asn55 and Glu85 has been implicated in controlling autodephosphorylation (42). Sequence alignment of CheYs showed that Thr84 is conserved within strains of *H. pylori* and in several species of *Epsilonproteobacteria* (Fig. 1). Thr84 Oγ in the β4-α4 loop is hydrogen bonded with BeF_3^- (3.50 Å), which may affect the phosphotransfer reaction. The role of Thr84 in HpCheY1 phosphorylation was investigated by introducing a Thr-to-Ala mutation, and phosphorylation of HpCheY1 by acetyl phosphate was measured by equilibrium titration (up to 10 mM). The T84A mutant had an approximately 4- to 5-fold (0.22 ± 0.055 mM) lower K_m value than that of the wild type (1.07 ± 0.31 mM) (Fig. 2B). The K_m value determined for HpCheY1 is comparable to the previously determined K_m value of EcCheY (3.2 ± 0.4 mM) (36). The lower K_m value for HpCheY1 may be due to the differences in ionic strength in the experiment performed (200 mM buffer salt used in the previous experiment, compared to 50 mM used in our experiment).

The K_m value is derived from the binding constant and rate constant ($K_m = K_s \cdot k_3/k_2$). A lower K_m value could be due to an increase in the binding affinity between CheY and the phosphodonor (smaller K_s), a faster rate of phosphorylation of bound CheY (larger k_2) or a slower rate of autodephosphorylation (smaller k_3) (36). It has been reported that Ala88 in EcCheY cannot be substituted for by amino acid residues with

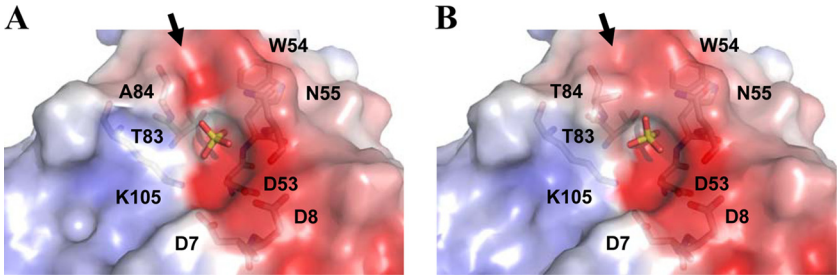

FIG. 5. Electrostatic surface representation with the contour level ± 5 kT/e showing the active-site pocket of SO_4^{2-}-bound HpCheY1/T84A (A) and SO_4^{2-}-bound HpCheY1 (B). The position of SO_4^{2-} is shown as a stick. Active-site residues are labeled. The arrow indicates the difference on the electrostatic surface between the two structures (see text). Electrostatic surfaces were calculated using the software APBS (3). Ligands were not included in the calculation.

long side chains (38). Multiple sequence alignment from various response regulators showed that Thr84 is most frequently replaced by small residues, including Ser, Ala, and Gly, and more rarely by hydrophobic Val and Ile (42). The structure of HpCheY1/T84A with SO_4^{2-} bound was almost identical to the wild type (CαRMSD = 0.1 Å), suggesting that the mutation would have no effect on backbone orientation. No significant difference around the active-site pocket was observed when comparing the surface electrostatic potential of wild-type HpCheY1 and the T84A mutant. A more electronegative surface was observed in the T84A mutant due to the exposed negative charge of Oγ of Thr83 (Fig. 5). Future study of the T84V mutant would provide insight into the role of the hydroxyl group in phosphorylation.

Comparison of the motor binding surfaces. Although HpCheY1 and EcCheY share high sequence identity and structural homology, we have noted a major difference at the FliM binding surface. The HpCheY1 structure differs from the EcCheY structure because of the upshift and shortening of helix 5 (Fig. 3A). We hypothesized that this structural difference would lead to a different CheY-FliM interaction in *H. pylori*. We examined the biological function of wild-type and mutant HpCheY1 in *E. coli* using a swarming assay. Bacterial swarming ability was assessed by transforming pTrc99a vectors encoding HpCheY1 and HpCheY1/D53A into wild-type *E. coli* (RP437) and into *cheY* (RP5232)- and *cheZ* (RP1616)-null mutants (Fig. 6). A control experiment using the empty pTrc99a vector was also conducted. Our results show that expression of HpCheY1 did not restore swarming of the *cheY*-null *E. coli* mutant. On the other hand, HpCheY1 inhibited swarming of wild-type *E. coli* in an IPTG concentration-dependent manner, suggesting that HpCheY1 associates with the *E. coli* chemotaxis system. Surprisingly, the expression of the HpCheY1/D53A mutant, a nonphosphorylatable mutant, inhibited *E. coli* swarming but did not affect cell growth. This result is different from that obtained by Alexandre et al. (1), who demonstrated that the heterologous expression of a wild-type CheY homolog from *Azospirillum brasilense*, but not the active-site mutant, inhibited the swarming of *E. coli*. Our results suggest that HpCheY1/D53A may interact with the chemotactic system of *E. coli*. Heterologous expression of CheY homologs from *Rhodobacter sphaeroides* partially restored *cheZ*-null mutant swarming, suggesting that CheY, with no motor binding affinity, competes with EcCheY for phosphate (35). In our study, HpCheY1, but not HpCheY1/D53A, restored the swarming ability of the *cheZ*-null mutant. It is possible that phosphorylation ability is necessary to bring the run-to-tumble ratio of the *cheZ*-null mutant close to that of the wild type. Wild-type HpCheY1, but not the D53A mutant, was able to receive a phosphate from EcCheA to modulate the concentration of EcCheY-P, therefore controlling the run-to-tumble ratio. Similar effects have also been observed in heterologous gene expression experiments using HpCheV2 and HpCheV3 (31). HpCheY1 failed to restore swarming of the *cheY*-null mutant, suggesting that HpCheY1 does not interact with EcFliM, even though HpCheY1 can be phosphorylated by EcCheA.

Sequence alignment between HpCheY1 and EcCheY suggested that the hydrophobic residues in α4 and β5 that are involved in $FliM_{NM}$ binding are either identical in the two proteins or are replaced by residues with similar amino acid properties (Fig. 1). However, salt bridge formation between the residues in helix 5 and the EcFliM peptide was disrupted (between the Asp12 Oδ of EcFliM-Lys119 and Nζ of EcCheY and between the Asn16 carboxylate of EcFliM-Lys122 and Nζ of EcCheY) (21). Although Lys119 of EcCheY is conserved in HpCheY1 (Lys115), the upshift of helix 5 caused displacement of Lys by a distance of approximately 4.4 Å (the distance between the Cα atom of Lys 115 in HpCheY and that of the equivalent Cα in EcCheY). Additionally, it was noted that the FliM-interacting α4/β5/α5 surface is more hydrophobic in HpCheY1. Specifically, the corresponding position of Lys122 in EcCheY is occupied by Val118 in HpCheY1 (Fig. 3A). Results of pull-down experiments from us and from Lowenthal et al. (23) show that HpCheY1-HpFliM interaction could be detected only if the concentration of KCl in the binding buffer was higher than 250 mM, while EcCheY1-EcFliM interaction was detected with no NaCl/KCl added (46). We speculated that the HpCheY1-HpFliM interaction would involve more extensive hydrophobic interactions. Sequence alignment of HpFliM and EcFliM revealed that the N-terminal fragments responsible for the interactions with CheY differ by four residues (G2A, S4-*del*, A9E, and N16E). It is likely that the interaction in *H. pylori* would be different from that in *E. coli*.

HpCheA-P2 preferentially interacts with HpCheY1. One of the distinctive features of the *H. pylori* chemotactic pathway is the presence of a CheY-like domain fused to CheA (HpCheAY2); another distinctive feature is the presence of three CheV proteins. An *in vitro* experiment showed that HpCheA displayed a higher preference for HpCheY1 than HpCheY2; HpCheA had the low-

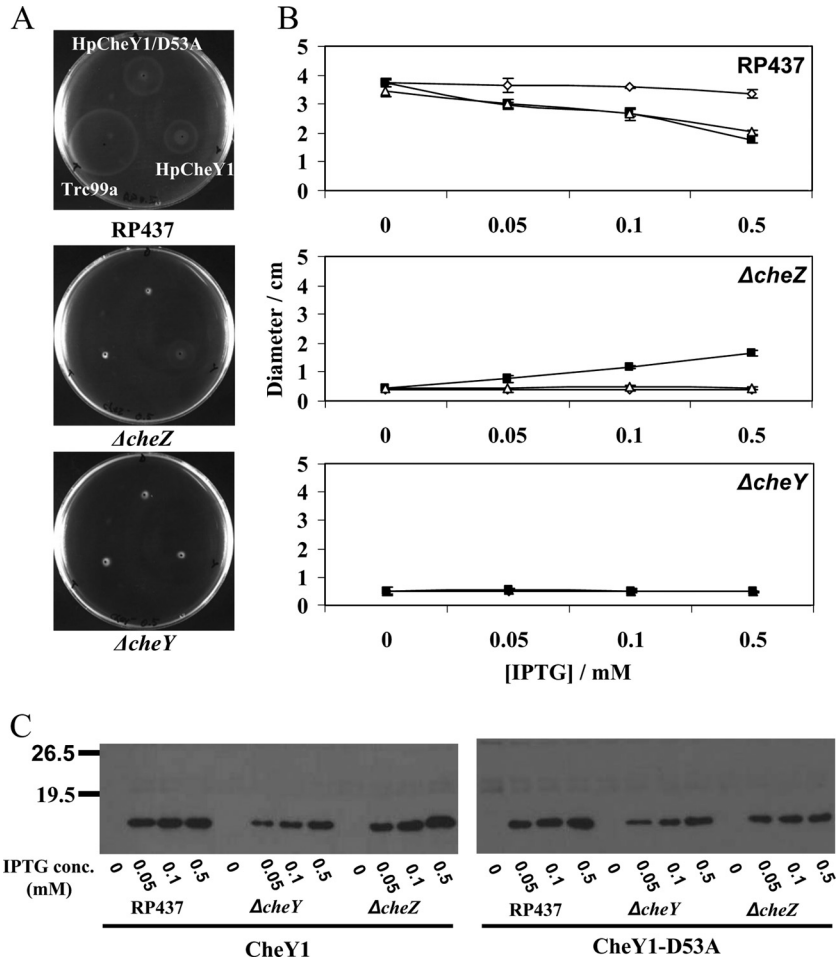

FIG. 6. Swarming motility assay of heterologous expression of HpCheY1 and HpCheY1-D53A in the *E. coli* wild type (RP437) and *cheZ* (RP1616)- and *cheY* (RP5232)-null mutants. Overnight cultures of cells carrying plasmids were inoculated onto TB–0.4% semisolid agar plates that were incubated at 30°C for 7 h. (A) Representative images of the swarming rings produced from the expression of pTrc99a (control), HpCheY1, or HpCheY1/D53A in 0.5 mM IPTG are shown. (B) Mean diameters of the rings are plotted against IPTG concentrations. The experiment was replicated 3 times. ◇, pTrc99a; ■, HpCheY1; △, HpCheY1-D53A. (C) Protein expression levels of HpCheYs in *E. coli* wild-type and mutant strains were probed by anti-HpCheY1 antibody.

est preference for the HpCheV proteins (15). The P2 domain in CheA consists of a docking site for response regulators and serves to increase the rate of phosphotransfer by concentrating CheY near P1 (14). We suspected that the binding affinities of response regulators for HpCheA-P2 would contribute to the differential rate of phosphotransfer in *H. pylori*. Interaction of HpCheA-P2 with the HpCheY and HpCheV proteins was investigated by a pull-down experiment and by gel filtration analysis.

Recombinant HpCheA-P2-His_8, HpCheY1, HpCheY2, HpCheV1, HpCheV2, and HpCheV3 were purified to greater than 95% purity. HpCheA-P2 was immobilized on Ni-NTA resin, followed by incubation with HpCheYs or HpCheVs. As shown in Fig. 7A, only HpCheY1 was shown to interact with HpCheA-P2, suggesting that HpCheY1 is the sole interacting partner of HpCheA-P2. The interaction between HpCheY1 and HpCheA-P2 was further investigated by gel filtration analysis. HpCheA-P2 and HpCheY1 were eluted at 14.57 ml and 16.05 ml, respectively, when run individually. When the two proteins were mixed and then subjected to the gel filtration analysis, the elution profile was shifted to 12.89 ml. Complex formation was further verified by SDS-PAGE analysis (Fig. 7B). Our results suggest that CheY1 formed a stable complex with CheA-P2. When the experiment was repeated with CheV3 and CheA-P2, the elution profile of the CheV3–CheA-P2 mixture did not change as compared to the elution profiles of the individual proteins (data not shown). We attempted to identify the surface of CheA-P2 that interacts with CheVs by homology modeling using Modeler (34). CheV3 was chosen as the representative CheV because it shares the highest sequence identity with HpCheY1. The P2 interaction patch on the α4/β5/α5 surface of HpCheV3 was found to be more electronegative than those of EcCheY and HpCheY1 (data not shown).

The high binding affinity of HpCheY1 for HpCheA-P2 observed in the present study is consistent with previous results showing that HpCheA has a greater phosphotransfer efficiency to HpCheY1 (15). Our data further suggest that the differential phosphotransfer efficiency is regulated by the interaction between the HpCheY/HpCheV proteins and the CheA-P2 domain. The P2 domain stands out because of its low sequence conservation among other regions of CheA, and HpCheA-P2

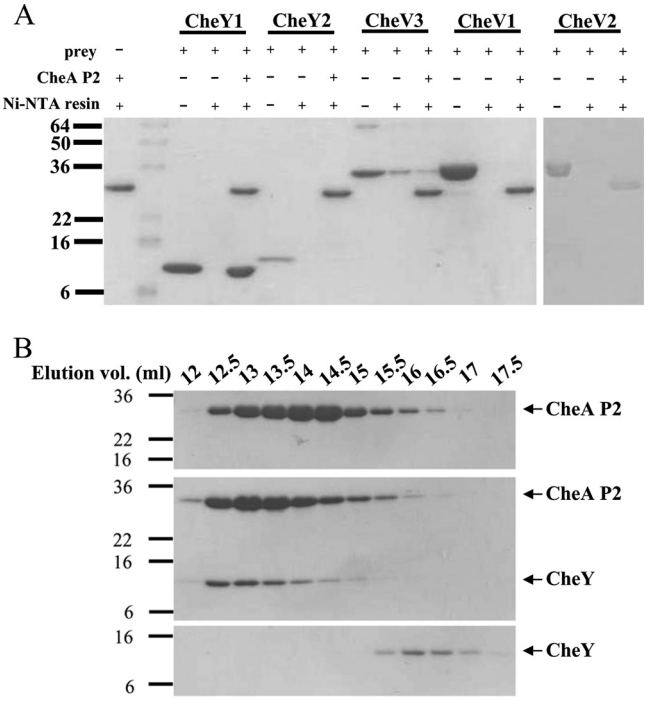

FIG. 7. Interaction study of HpCheA-P2 and HpCheYs/CheVs. (A) Purified CheA-P2 in 0.1 mg/ml was immobilized. Response regulators in a 1:1 molar ratio to CheA-P2 were then added and incubated at 4°C for 1 h. After washing, the beads were boiled at 90°C and loaded for SDS-PAGE. (B) Elution profiles of CheY1 (lower panel), P2 (upper panel), and the CheY1-P2 complex (middle) separated by 10/30 Superdex 200 size exclusion chromatography. The elution volume is indicated above the graph. The elution volumes of P2, CheY1, and the CheY1-P2 complex are 14.57 ml, 16.05 ml, and 12.89 ml, respectively.

only shares 15% sequence identity with EcCheA-P2. In fact, the regulation would be complicated in HpCheV proteins, as the N-terminal CheW-like domain may interact with the P5 regulatory domain of CheA and affect the phosphotransfer activity. How this interaction affects the phosphotransfer reaction remains unclear. Structure determination studies of other CheY-like domains and of their complexes with CheA would help us unravel the complex regulatory mechanisms underlying the chemotactic network in *H. pylori*.

ACKNOWLEDGMENTS

We thank John S. Parkinson for providing the *E. coli* mutants.

This work was supported by a Competitive Earmarked Research Grant (CUHK 4592/06 M) from the Research Grants Council of Hong Kong.

REFERENCES

1. **Alexandre, G., and I. B. Zhulin.** 2003. Different evolutionary constraints on chemotaxis proteins CheW and CheY revealed by heterologous expression studies and protein sequence analysis. J. Bacteriol. **185:**544–552.
2. **Alm, R. A., L. S. Ling, L. D. T. Moir, et al.** 1999. Genomic-sequence comparison of two unrelated isolates of the human gastric pathogen *Helicobacter pylori*. Nature **397:**176–180.
3. **Baker, N. A., D. Sept, S. Joseph, M. J. Holst, and J. A. McCammon.** 2001. Electrostatics of nanosystems: application to microtubules and the ribosome. Proc. Natl. Acad. Sci. U. S. A. **98:**10037–10041.
4. **Cho, H. S., S. Y. Lee, D. Yan, X. Pan, J. S. Parkinson, S. Kustu, D. E. Wemmer, and J. G. Pelton.** 2000. NMR structure of activated cheY. J. Mol. Biol. **297:**543–551.
5. **Collaborative Computational Project, Number 4.** 1994. The CCP4 suite: programs for protein crystallography. Acta Crystallogr. D Biol. Crystallogr. **50:**760–763.
6. **Covacci, A., J. L. Telford, G. Del Giudice, J. Parsonnet, and R. Rappuoli.** 1999. *Helicobacter pylori* virulence and genetic geography. Science **284:**1328–1333.
7. **DeLano, W. L.** 2002. The PyMOL molecular graphics system. DeLano Scientific, San Carlos, CA.
8. **Dyer, C. M., and F. W. Dahlquist.** 2006. Switched or not? The structure of unphosphorylated CheY bound to the N terminus of FliM. J. Bacteriol. **188:**7354–7363.
9. **Dyer, C. M., M. L. Quillin, A. Campos, J. Lu, M. M. McEvoy, A. C. Hausrath, E. M. Westbrook, P. Matsumura, B. W. Matthews, and F. W. Dahlquist.** 2004. Structure of the constitutively active double mutant CheYD13KY106W alone and in complex with a FliM Peptide. J. Mol. Biol. **342:**1325–1335.
10. **Dyer, C. M., A. S. Vartanian, H. Zhou, and F. M. Dahlquist.** 2009. A molecular mechanism of bacterial flagellar motor switching. J. Mol. Biol. **338:**71–84.
11. **Eaton, K. A., S. Suerbaum, C. Josenhans, and S. Krakowka.** 1996. Colonization of gnotobiotic piglets by *Helicobacter pylori* deficient in two flagellin genes. Infect. Immun. **64:**2445–2448.
12. **Emsley, P., and K. Cowtan.** 2004. Coot: model-building tools for molecular graphics. Acta Crystallogr. D Biol. Crystallogr. **60:**2126–2132.
13. **Holm, L., S. Kaariainen, P. Rosenstrom, and A. Schenkel.** 2008. Searching protein structure databases with DaliLite v. 3. Bioinformatics **24:**2780–2781.
14. **Jahreis, K., T. B. Morrison, A. Garzón, and J. S. Parkinson.** 2004. Chemotactic signaling by an *Escherichia coli* CheA mutant that lacks the binding domain for phosphoacceptor partners. J. Bacteriol. **186:**2664–2672.
15. **Jiménez-Pearson, M. A., I. Delany, V. Scarlato, and D. Beier.** 2005. Phosphate flow in the chemotactic response system of *Helicobacter pylori*. Microbiology **151:**3299–3311.
16. Reference deleted.
17. **Kavermann, H., B. P. Burns, K. Angermuller, S. Odenbreit, W. Fischer, K. Melchers, and R. Haas.** 2003. Identification and characterization of *Helicobacter pylori* genes essential for gastric colonization. J. Exp. Med. **197:**813–822.
18. **Larkin, M. A., G. Blackshields, N. P. Brown, R. Chenna, P. A. McGettigan, H. McWilliam, F. Valentin, I. M. Wallace, A. Wilm, R. Lopez, J. D. Thompson, T. J. Gibson, and D. G. Higgins.** 2007. ClustalW and ClustalX version 2. Bioinformatics **23:**2947–2948.
19. **Laskowski, R. A., M. W. MacArthur, and J. M. Thornton.** 1998. Validation of protein models derived from experiment. Curr. Opin. Struct. Biol. **8:**631–639.
20. **Lee, S. Y., H. S. Cho, J. G. Pelton, D. Yan, E. A. Berry, and D. E. Wemmer.** 2001. Crystal structure of activated CheY. Comparison with other activated receiver domains. J. Biol. Chem. **276:**16425–16431.
21. **Lee, S. Y., H. S. Cho, J. G. Pelton, D. Yan, R. K. Henderson, D. S. King, L. Huang, S. Kustu, E. A. Berry, and D. E. Wemmer.** 2001. Crystal structure of an activated response regulator bound to its target. Nat. Struct. Biol. **8:**52–56.
22. **Leslie, A.** 1995. MOSFLM users guide. MRC Laboratory of Moelcular Biology Cambridge, United Kingdom.
23. **Lowenthal, A. C., M. Hill, L. K. Sycuro, K. Mehmood, N. R. Salama, and K. M. Ottemann.** 2009. Functional analysis of the *Helicobacter pylori* flagellar switch proteins. J. Bacteriol. **191:**7147–7156.
24. **Lowenthal, A. C., C. Simon, A. S. Fair, K. Mehmood, K. Terry, S. Anastasia, and K. M. Ottemann.** 2009. A fixed-time diffusion analysis method determines that the three cheV genes of *Helicobacter pylori* differentially affect motility. Microbiology **55:**1181–1191.
25. **Lukat, G. S., W. R. McCleary, A. M. Stock, and J. B. Stock.** 1992. Phosphorylation of bacterial response regulator proteins by low molecular weight phospho-donors. Proc. Natl. Acad. Sci. U. S. A. **89:**718–722.
26. **McCoy, A. J., R. W. Grosse-Kunstleve, P. D. Adams, M. D. Winn, L.C. Storoni, and R. J. Read.** 2007. *Phaser* crystallographic software. J. Appl. Crystallogr. **40:**658–674.
27. **McGee, D. J., M. L. Langford, E. L. Watson, J. E. Carter, Y. T. Chen, and K. M. Ottemann.** 2005. Colonization and inflammation deficiencies in Mongolian gerbils infected by *Helicobacter pylori* chemotaxis mutants. Infect. Immun. **73:**1820–1827.
28. **Miller, L. D., M. H. Russell, and G. Alexandre.** 2009. Diversity in bacterial chemotactic responses and niche adaptation. Adv. Appl. Microbiol. **66:**53–75.
29. **Parkinson, J. P.** 1978. Complementation analysis and deletion mapping of *Escherichia coli* mutants defective in chemotaxis. J. Bacteriol. **135:**45–53.
30. **Pazy, Y., A. C. Wollish, S. A. Thomas, P. J. Miller, E. J. Collins, R. B. Bourret, and R. E. Silversmith.** 2009. Matching biochemical reaction kinetics to the timescales of life: structural determinants that influence the autodephosphorylation rate of response regulator proteins. J. Mol. Biol. **392:**1205–1220.
31. **Pittman, M. S., M. Goodwin, and D. J. Kelly.** 2001. Chemotaxis in the human gastric pathogen *Helicobacter pylori*: different roles for CheW and the three CheV paralogues, and evidence for CheV2 phosphorylation. Microbiology **147:**2493–2504.

32. **Rao, C. V., G. D. Glekas, and G. W. Ordal.** 2008. The three adaptation systems of *Bacillus subtilis* chemotaxis. Trends Microbiol. **16:**480–487.
33. **Riepl, H., B. Scharf, R. Schmitt, H. R. Kalbitzer, and T. Maurer.** 2004. Solution structures of the inactive and BeF3-activated response regulator CheY2. J. Mol. Biol. **338:**287–297.
34. **Sali, A., and T. L. Blundell.** 1993. Comparative protein modelling by satisfaction of spatial restraints. J. Mol. Biol. **234:**779–815.
35. **Shah, D. S., S. L. Porter, D. C. Harris, G. H. Wadhams, P. A. Hamblin, and J. P. Armitage.** 2000. Identification of a fourth cheY gene in *Rhodobacter sphaeroides* and interspecies interaction within the bacterial chemotaxis signal transduction pathway. Mol. Microbiol. **35:**101–112.
36. **Silversmith, R. E., J. L. Appleby, and R. B. Bourret.** 1997. Catalytic mechanism of phosphorylation and dephosphorylation of CheY: kinetic characterization of imidazole phosphates as phosphodonors and the role of acid catalysis. Biochemistry **36:**14965–14974.
37. **Silversmith, R. E., J. G. Smith, G. P. Guanga, J. T. Les, and R. B. Bourret.** 2001. Alteration of a nonconserved active site residue in the chemotaxis response regulator cheY affects phosphorylation and interaction with cheZ. J. Biol. Chem. **276:**18478–18484.
38. **Smith, J. G., J. A. Latiolais, G. P. Guanga, S. Citineni, R. E. Silversmith, and R. B. Bourret.** 2003. Investigation of the role of electrostatic charge in activation of the *Escherichia coli* response regulator CheY. J. Bacteriol. **185:**6385–6391.
39. **Szurmant, H., and G. W. Ordal.** 2004. Diversity in chemotaxis mechanisms among the bacteria and archaea. Microbiol. Mol. Biol. Rev. **68:**301–319.
40. **Terry, K., A. C. Go, and K. M. Ottemann.** 2006. Proteomic mapping of a suppressor of non-chemotactic cheW mutants reveals that *Helicobacter pylori* contains a new chemotaxis protein. Mol. Microbiol. **61:**871–882.
41. **Terry, K., S. M. Williams, L. Connolly, and K. M. Ottemann.** 2005. Chemotaxis plays multiple roles during *Helicobacter pylori* animal infection. Infect. Immun. **73:**803–811.
42. **Thomas, S. A., J. A. Brewster, and R. B. Bourret.** 2008. Two variable active site residues modulate response regulator phosphoryl group stability. Mol. Microbiol. **69:**453–465.
43. **Uemura, N., S. Okamoto, S. Yamamoto, N. Matsumura, S. Yamaguchi, M. Yamakido, K. Taniyama, N. Sasaki, and R. J. Schlemper.** 2001. *Helicobacter pylori* infection and the development of gastric cancer. N. Engl. J. Med. **345:**784–789.
44. **Volz, K., and P. Matsumura.** 1991. Crystal structure of *Escherichia coli* CheY refined at 1.7-Å resolution. J. Biol. Chem. **266:**15511–15519.
45. **Wadhams, G. H., and J. P. Armitage.** 2004. Making sense of it all: bacterial chemotaxis. Nat. Rev. Mol. Cell Biol. **5:**1024–1037.
46. **Welch, M., K. Oosawa, S. Aizawa, and M. Eisenbach.** 1993. Phosphorylation-dependent binding of a signal molecule to the flagellar switch of bacteria. Proc. Natl. Acad. Sci. U. S. A. **90:**8787–8791.
47. **Williams, S. M., Y. T. Chen, T. M. Andermann, J. E. Carter, D. J. McGee, and K. M. Ottemann.** 2007. *Helicobacter pylori* chemotaxis modulates inflammation and bacterium-gastric epithelium interactions in infected mice. Infect. Immun. **75:**3747–3757.
48. **Xu, Z., and S. W. Au.** 2005. Mapping residues of SUMO precursors essential in differential maturation by SUMO-specific protease, SENP1. Biochem. J. **386:**325–330.
49. **Yan, D., H. S. Cho, C. A. Hastings, M. M. Igo, S. Y. Lee, J. G. Pelton, V. Stewart, D. E. Wemmer, and S. Kustu.** 1999. Beryllofluoride mimics phosphorylation of NtrC and other bacterial response regulators. Proc. Natl. Acad. Sci. U. S. A. **96:**14789–14794.